IOP Conference Series: Materials Science and Engineering

OPEN ACCESS

Beamforming method based on phase dispersion Fourier analysis for SAFT images

To cite this article: D Romero-Laorden *et al* 2012 *IOP Conf. Ser.: Mater. Sci. Eng.* **42** 012009

View the article online for updates and enhancements.

You may also like

- Brought to Light. I. Quantification of Disk Substructure in Dwarf Early-type Galaxies
Josefina Michea, Anna Pasquali, Rory Smith et al.
- BROADBAND TURBULENT SPECTRA IN GAMMA-RAY BURST LIGHT CURVES
Maurice H. P. M. van Putten, Cristiano Guidorzi and Filippo Frontera
- Bar Classification Based on the Potential Map
Yun Hee Lee, Myeong-Gu Park, Hong Bae Ann et al.

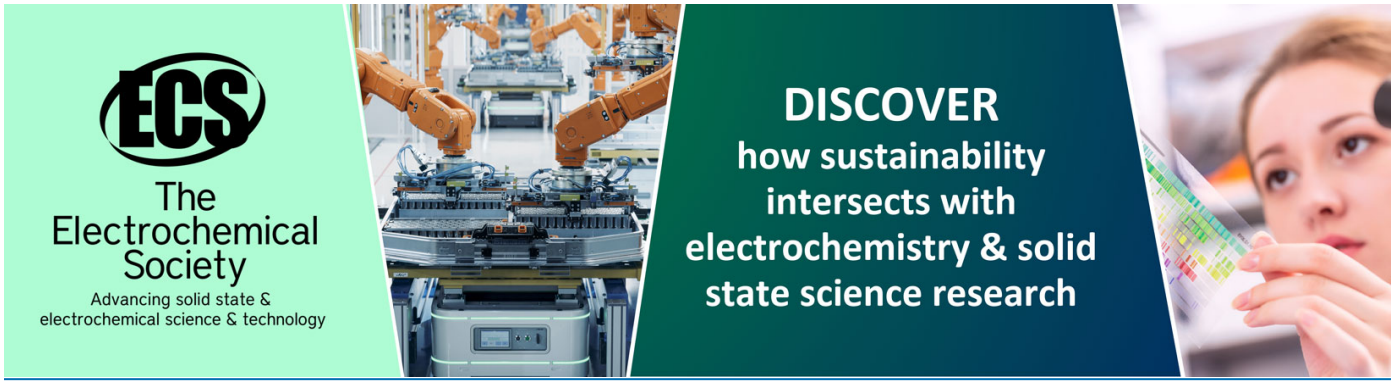

This content was downloaded from IP address 18.226.169.94 on 26/04/2024 at 14:46

IOP Conf. Series: Materials Science and Engineering **42** (2012) 012009 doi:10.1088/1757-899X/42/1/012009

Beamforming method based on phase dispersion Fourier analysis for SAFT images

D. Romero-Laorden, O. Martínez-Graullera, A. Ibañez and L. G. Ullate

Centro de Acústica Aplicada y Evaluación no Destructiva (CSIC-UPM)

E-mail: david.romero@csic.es

Abstract. A phase coherence descriptor based on the Fourier analysis of phase dispersion in ultrasound data is proposed. It can be easily computed and introduced as a ponderation factor during a traditional beamforming process. Theoretical and experimental results show that, for a linear array of 64 elements operating in Synthetic Aperture Techniques, the dynamic range is enhanced reaching up to 30dB.

1. Introduction

Synthetic Aperture Focusing Techniques (SAFT) have been a topic deeply studied in several areas such as radar, sonar or ultrasonic imaging. They are a very good solution to reduce the hardware requisites and consequently the consumption and cost of the systems, making possible their miniaturization and portability.

However, beamforming in SAFT is a highly data parallel process that can be easily pipelined and executed on a single GPU or several of them. Nowadays GPU beamformers are a reality [1], but their use in real time is limited by some factors. A Full Matrix Array capture (FMA) is used to obtain the complete set of signals and after the acquisition a Total Focusing Method (TFM) is applied to generate an image [2]. Supposing an array of N elements it means to process $N \times N$ signals. Therefore, TFM requires a high number of signals what increase the cost involved in the acquisition system, the data transfer and the computational cost. In order to develop real time imaging systems, the solution relative to this problem is to employ acquisition methods based on solutions of minimum redundancy (coarray-based). The simplest is the technique known as 2R-SAFT which significantly reduces the number of electronic channels and provides images with good quality and grating lobes free [3]. Furthermore, coarray-based implementations with GPGPU techniques achieves an speed up of 150x [1] over CPU beamforming.

The problem is that dynamic range is compromised because coarray-based methods involve only $(2N - 1)$ signals compared to the TFM which involves $(N \times N)$. This paper proposes the use with minimum redundancy solutions, of a new coherence factor map based on a descriptor of Fourier Series to enhance the dynamic range, reaching the image quality of the TFM.

2. Minimum redundancy approach

We have chosen a method of minimum redundancy suggested in [4] (we will refer it as FnR SAFT as abbreviation) where each element of the "effective aperture" or coarray is composed

by only a signal, working with a reduced set of parallel channels. Supposing $N_e = \frac{2N}{Nc}$ the number of elements in emission, the i-emitter is defined as

$$\hat{e}_i = \frac{N_c}{2} i \qquad i = [1 : N_e] \quad / \quad 1 \leq \hat{e}_i \leq N \tag{1}$$

where N_c is the number of parallel channels operating in reception and N is the number of array elements. Similarly, we describe the k-receiver as:

$$\hat{r}_k = \hat{e}_i + k - \frac{N_c}{2} \qquad k = [1 : N_c] \quad / \quad 1 \leq \hat{r}_k \leq N \tag{2}$$

For convenience, suppose $X_{\hat{e},\hat{r}}(t)$ the number of signals acquired expressed in-phase I and quadrature components Q:

$$X_{\hat{e},\hat{r}}(t) = I_{\hat{e},\hat{r}}(t) + jQ_{\hat{e},\hat{r}}(t) = \mathbf{X}_{\hat{e},\hat{r}}(t) e^{j\phi_{\hat{e},\hat{r}}(t)} \tag{3}$$

where $X_{\hat{e},\hat{r}}(t)$ is the signal, obtained by the emitter $\hat{e}$ and receptor $\hat{r}$. Then $\mathbf{X}_{\hat{e},\hat{r}}(t)$ is the modulus and $\phi_{\hat{e},\hat{r}}(t)$ its corresponding signal phase. According to this expression and relative to the method mentioned in this work, the FnR image $A(\vec{x})$ can be calculated as:

$$A(\vec{x}) = \sqrt{\left(\sum_{i=1}^{N_e}\sum_{k=1}^{N_c} I_{\hat{e}_i,\hat{r}_k}(T(\vec{x}))\right)^2 + \left(\sum_{i=1}^{N_e}\sum_{k=1}^{N_c} Q_{\hat{e}_i,\hat{r}_k}(T(\vec{x}))\right)^2} \tag{4}$$

where $T(\vec{x})$ is the focussing delay for the $\vec{x} = (x, z)$ point which compensates emission and reception distances:

$$T(\vec{x}) = \frac{\sqrt{(x - x_{\hat{e}})^2 + z^2} + \sqrt{(x - x_{\hat{r}})^2 + z^2}}{c} \tag{5}$$

being $x_{\hat{e}}$ and $x_{\hat{r}}$ the coordinates of the elements $\hat{e}$ and $\hat{r}$, and (x, z) the space point.

3. Coherence Factor Map Image

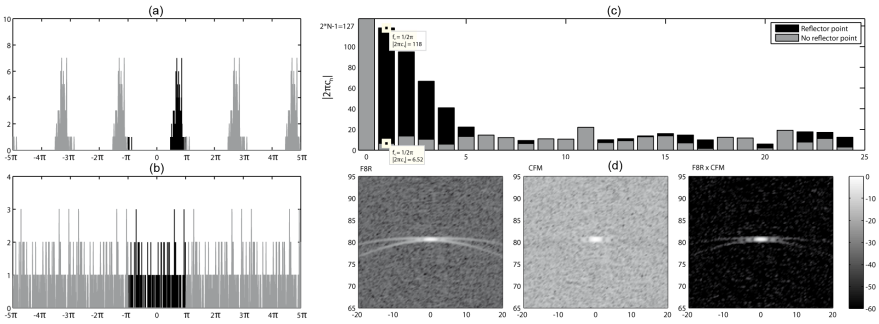

Figure 1. (a) $P(\phi)$ and $\Phi(\phi)$ in a point near to the reflector; (b) $P(\phi)$ and $\Phi(\phi)$ in a no reflector point; (c) 24 coefficients of Fourier series for both points, the component $f_\phi = \frac{1}{2\pi}$ has been remarked; (d) The images of the reflector point for F8R, CFM and F8R×CFM.

In general, coherence-based methods weight each image point according to the coherence estimated from the receive aperture domain data [5, 6]. As Delay and Sum beamforming, the coherence based beamformer is a non-adaptive tool based on the fact that element-signal-data from the mainlobe region are coherent, whereas those from the sidelobe region are incoherent.

Once the delays corresponding to each signal have been applied, at each image point a set of signal phases is obtained to compose a phase distribution function by a sum of Kronecker deltas:

$$P(\phi) = \sum_{i=1}^{N_e} \left(\sum_{k=1}^{N_c} \delta[\phi - \phi_{\hat{e}_i,\hat{r}_k} T(\vec{x}))] \right) \tag{6}$$

where $\phi_{\hat{e}_i,\hat{r}_k}(T(\vec{x}))$ is the phase of the signal emitted by $\hat{e}_i$-element and received by $\hat{r}_k$-element compensated at (x, z). These values are distributed in the $[-\pi, \pi]$ interval and can be extended to form the periodic signal using a comb-function based on Dirac deltas:

$$\Phi(\phi) = \sum_{m=-\infty}^{\infty} \delta(\phi - m2\pi) * P(\phi) \tag{7}$$

Figure 1 shows two image points in a simulated medium. A 64-element linear array has been simulated with 127 signals (F8R with 30% of noise).In a point near to the reflector position phases are concentrated (figure 1(a)), and a location where there is no reflector (figure 1(b)) showing an uniform distribution in the $[-\pi, \pi]$ range. The periodic extension of $P(\phi)$ can be decomposed by Fourier Series into a sum of simple oscillating functions:

$$c_n = \frac{1}{2\pi} \int_{-\pi}^{\pi} \Phi(\phi) e^{-j2\pi n f_o \phi} d\phi = \frac{1}{2\pi} \sum_{i=1}^{N_e} \left(\sum_{k=1}^{N_c} e^{-j2\pi n f_o \phi_{\hat{e}_i,\hat{r}_k}(T(\vec{x}))} \right) \tag{8}$$

where, according to the signal period, $f_o = \frac{1}{2\pi}$. Figure 1(c) shows the values of c_n for the first 24 sinusoidal components of the Fourier series. If the signal $P(\phi)$ is composed by a random distribution of phases its energy is spread over all the Fourier Coefficients which are low valued. However, when there is a concentration of phases it increases the presence of the sinusoidal components of period $\frac{1}{2\pi}$ than can be evaluated easily if $n = 1$ (equation (8)). Then, our coherence factor at point (x, z) is defined as:

$$C_1(\vec{x}) = (2\pi)c_1 = \sum_{i=1}^{N_e} \sum_{k=1}^{N_c} e^{-j\phi_{\hat{e}_i,\hat{r}_k}(T(\vec{x}))} = \sum_{i=1}^{N_e} \sum_{k=1}^{N_c} \frac{I_{\hat{e}_i,\hat{r}_k}(T(\vec{x}))}{\mathbf{X}_{\hat{e}_i,\hat{r}_k}(T(\vec{x}))} - j \sum_{i=1}^{N_e} \sum_{k=1}^{N_c} \frac{Q_{\hat{e}_i,\hat{r}_k}(T(\vec{x}))}{\mathbf{X}_{\hat{e}_i,\hat{r}_k}(T(\vec{x}))} \tag{9}$$

The maximum value of this function is achieved when all phase components are concentrated and is ($2N - 1$, 127 in this case), which is the total number of signals involved in the process. In figure 1 the coherence has been measured at the reflector point that is contributed by 118 signals (figure 1(a)), and in the point where there is no reflector the coherence is reduced to be composed by only 6 signals (figure 1(b)).

The complete image Coherence Factor Map (CFM) can be expressed then by:

$$H(\vec{x}) = \sqrt{\left(\sum_{i=1}^{N_e} \sum_{k=1}^{N_c} \frac{I_{\hat{e}_i,\hat{r}_k}(T(\vec{x}))}{\mathbf{X}_{\hat{e}_i,\hat{r}_k}(T(\vec{x}))} \right)^2 + \left(\sum_{i=1}^{N_e} \sum_{k=1}^{N_c} \frac{Q_{\hat{e}_i,\hat{r}_k}(T(\vec{x}))}{\mathbf{X}_{\hat{e}_i,\hat{r}_k}(T(\vec{x}))} \right)^2} \tag{10}$$

Using it with $A(\vec{x})$ (equation (4)) the new image equation is then $I(\vec{x}) = A(\vec{x})H(\vec{x})$.

4. Experimental Results

As an experimental procedure a tissue phantom (Model 040GSE - CIRS Inc.) with a 0.5dB/MHzcm attenuation, and 0.1mm diameter wires was examined using a 2.6MHz phased array transducer of $N = 64$ elements, 0.28mm of pitch. The figure 2 shows a line of 11 wires (covering an area starting at 17 to 122mm depth). The TFM image was composed for the DAS algorithm using the complete set of signals ($N \times N = 4096$). Next, F8R and Coherence Factor Map were calculated for the case of $N_c = 8$ using 127 signals ($2N - 1$). According to our

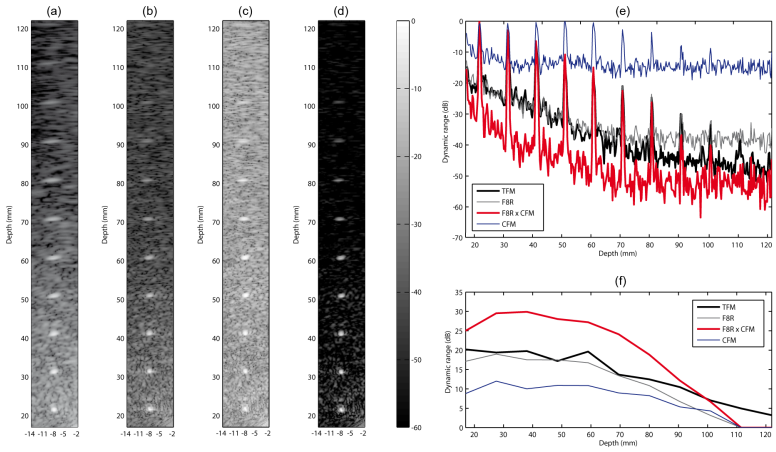

Figure 2. Experimental images of a line of wires in a tissue phantom. (a) TFM, (b) F8R, (c) CFM, (d) F8R×CFM; (e) Lateral profile in deep; (f) Variation of dynamic range in deep.

calculations and compared with 2R-SAFT, working with a strategy of minimum redundancy as F8R reduce 20% the acquisition time.

Corresponding images relative to TFM, F8R, CFM and F8R×CFM are represented in figures 2(a)(b)(c)(d) respectively. Original A-Scan has a SNR of 12dB for the highest echo. As we can observe, TFM image shows 11 wires, the SNR at each deep remains constant to 20dB until 60mm, then it decreases to 5dB at 120mm (figure 2(f)). The F8R image shows only 9 wires, with a constant local SNR of 17dB until 60mm, disappearing the echo response at positions upper to 100mm. The CFM image shows 9 wires however the coherence is reduced for positions upper to 80mm and it is lost for positions upper to 100mm. The combination of CFM and F8R produces a SNR that raises values of 30dB and is maintained upper than TFM until 100mm.

5. Conclusions

A new descriptor based on phase dispersion has been presented with the goal of increasing the dynamic range in SAFT images. Experimental results have validated our method and it has been shown that its implementation is extremely simple. The method has shown that it is robust against noise and attenuation. The CFM maintains a constant SNR in a large region of the image that produces, for the F8R×CFM, better results than TFM in the 80% of the image, being finally limited by the SNR in the F8R image. This problem can be coped with pulse code compression techniques, and different options to combine it with CFM are now under study.

Acknowledgements

This work has been supported by the Spanish Ministry of Economy in project DPI2010-19376.

References

[1] Romero-Laorden D, Martínez-Graullera O, Martín-Arguedas C J, Tokio Higuti R and Octavio A 2009 *IEEE Ultrason. Symp.* (Rome, Italy, 20-23 September 2009) pp 1334–1337
[2] Holmes C, Bruce W Drinkwater and Wilcox P D 2005 *NDT & E International* **38** 701–711
[3] Martín-Arguedas C J, Martínez-Graullera O and Ullate L G 2008 *IEEE Ultrason. Symp.* (Beijing, China, 2-5 November 2008) pp 721–724
[4] Lockwood G R, Li P C, O'Donnell M and Foster F S 1996 *IEEE Trans. Ultrason. Ferro. Freq.Contr* **43** 7–14
[5] Hollman K W, Rigby K W and O'Donnell M 1999 *IEEE Ultrason.Symp.* (Caesars Tahoe, NV, 17-20 October 1999) pp 1257–1260
[6] Camacho J, Parrilla M and Fritsch C 2009 *IEEE Trans. Ultrason. Ferro. Freq.Contr* **56** 958–74